Pyrolysis characteristics and kinetics of sour cherry stalk and flesh via thermogravimetric analysis using isoconversional methods

Gözde Gözke[1] · Korkut Açıkalın[2]

Abstract

Pyrolysis characteristics and kinetics of sour cherry stalk and flesh were investigated using non-isothermal thermogravimetric analysis at five different heating rates of 5, 10, 20, 30 and 40 °C min^{-1}. Activation energies at two different particle size ranges were determined from the experimental data using various isoconversional methods, namely Friedman, Flynn–Wall–Ozawa and Kissinger–Akahira–Sunose methods. Four stages were observed during the pyrolysis process in which the second and the third stage were determined as active decomposition stages. Average activation energies of sour cherry stalk with a particle size of 75–150 μm were calculated in the range of 159.0–160.5 kJ mol^{-1} and 118.8–141.1 kJ mol^{-1} at the second and the third active stage, respectively. The same type of biomass with a particle size of 150–250 μm revealed average activation energies in the range of 179.7–180.0 kJ mol^{-1} and 162.1–164.6 kJ mol^{-1} at the second and the third active stage, respectively. Average activation energies of sour cherry flesh with a particle size of 75–150 μm were calculated in the range of 136.2–160.5 kJ mol^{-1} and 133.7–151.2 kJ mol^{-1} at the second and the third active stage, respectively. The same type of biomass with a particle size of 150–250 μm resulted in average activation energies in the range of 266.1–273.9 kJ mol^{-1} and 179.8–197.8 kJ mol^{-1} at the second and the third active stage, respectively. Besides the obtained activation energy values, results demonstrated the effect of the particle size of the applied biomass on pyrolysis kinetics as well as the possibility of using sour cherry stalk and flesh as renewable feedstock for alternative energy source.

Keywords Sour cherry stalk · Sour cherry flesh · Pyrolysis kinetics · Isoconversional methods · Multistage process

Introduction

Increasing energy demand and the depletion of fossil fuels as well as environmental issues originating from the utilization of fossil fuels led an increase in the search of alternative energy sources [1]. Biomass being a renewable energy source has initiated a major interest over the past decades due to the advantages such as availability, sustainability and environment-friendly concerns [2]. In other words, biomass is available abundantly on earth while preserving essential ecosystem functions and can reduce the carbon dioxide concentration in the atmosphere and releases less sulfur and nitrogen oxides when used as combustion material [3].

Biomass originated energy covers a considerable amount of energy need in the world [4]. Main biomass sources include agricultural residues such as stalks, husks and straw; forest residues such as residual wastes from logging and thinning processes; waste of different origins such as from municipal, agricultural and industrial extractions; and energy crops such as oilseeds, sugar crops and algae [5]. Potential use of biomass as renewable energy resource depends on the feedstock properties and process parameters [6, 7].

Thermochemical conversion methods, such as pyrolysis, combustion and gasification, are the commonly preferred processes to produce energy from biomass. Among these methods, pyrolysis is the most preferred approach resulting from lower temperature requirement, lack of oxidizing agents in the process and higher quality final products compared with aforementioned methods [8]. Pyrolysis is a thermal degradation process in which biomass is converted into valuable biofuel in the absence of oxygen at a temperature range between 350 and 700 °C [9]. As a

✉ Gözde Gözke
  gozde.gozke@yalova.edu.tr

1 Department of Chemical Engineering, Faculty of Engineering, Yalova University, Yalova, Turkey

2 Department of Energy Systems Engineering, Faculty of Engineering, Yalova University, Yalova, Turkey

result of thermal decomposition, biomass is converted into carbon-rich solid product, an oil-like liquid product and a hydrocarbon-rich gaseous product [10]. For an adequate reactor design, large-scale development and optimization of thermochemical processes, pyrolysis kinetics needs to be known [11]. Thermogravimetric analysis (TGA) has become an effective tool for the investigation of pyrolysis kinetics along with the development of thermal analytical instruments. The mass change of biomass as a function of increasing temperature reveals essential information about reaction mechanism and kinetic parameters, i.e., apparent activation energy (E_a) and pre-exponential factor (A). These kinetic parameters together with reaction model are called as kinetic triplets [12].

Kinetic evaluation of TGA data can be performed basically by using two classes of methods: model-fitting (model based) methods and model-free (isoconversional) methods [13]. The model-fitting methods describe the pyrolysis process by fitting different reaction models. Corresponding kinetic parameters are calculated from the assumed reaction model. However, correct selection of appropriate reaction model is one of the difficult tasks to be fulfilled [14]. In contrast to model-fitting methods, isoconversional methods can estimate the kinetic parameters without assessing the reaction model. The possible errors which could arise from the assumed reaction model can be avoided by using isoconversional methods [15, 16].

Sour cherry (*Prunus cerasus* L.) belongs to the family of *Rosaceae* [17]. Owing to its specific flavor, sour cherries are one of the most popular fruits worldwide. Annual production capacity in the world is around 1.378.216 metric tonnes in 2016, while the leading producers are Russian Federation, Poland, Turkey and Ukraine with production yields of 16.72%, 14.13%, 13.96% and 11.35%, respectively [18]. The high production amount demonstrates the importance of the evaluation of sour cherry in different forms. The main application areas of sour cherries are in juice, wine and jam production for food industry [19–21]. Due to the consumer preferences in Turkey, 40% of total production of sour cherry is processed in juice production [20]. Relating to the fact that crucial part of the production is used for juice preparations, a considerable amount of pomace is produced.

Sour cherry flesh and stalk are generated as a residue of industrial processing of sour cherries for juice production. The studies that address the thermal behavior of cherry and sour cherry stones concern more likely the carbonization process [22–24]. Nevertheless, the pyrolysis of cherry stones was studied by several research groups [25–28]. However, there are a deficient number of studies related to thermal decomposition of sour cherry stones [29], and moreover, no studies about thermal behavior of sour cherry stalk and flesh, which is a by-product of sour cherry processing industry, have been conducted.

The present study investigates the thermal decomposition of sour cherry flesh and stalk via thermogravimetric analysis and estimates the activation energies by using three different isoconversional methods which are Friedman, Flynn–Wall–Ozawa and Kissinger–Akahira–Sunose method. The results disclose the pyrolysis kinetics and characteristics revealing proper design, optimization and modeling conditions of pyrolysis process.

Methods

Materials

Sour cherry pomace which consists of sour cherry flesh and stalk was used in thermogravimetric experiments, separately. Sour cherry pomace was provided by a fruit juice producing company, DİMES (İzmir, Turkey). The supplied material was firstly dried under sun for 2 weeks, and then, sour cherry flesh and stalks were separated. All the samples of sour cherry pomace were ground by using an analytic mill (IKA A11, Staufen im Breisgau, Germany) and sieved to the particle size of two different fractions, 75–150 μm and 150–250 μm. The samples were dried in an oven at 105 °C for 12 h to remove moisture and kept in glass containers after being stored in desiccator for 24 h. The fractions were then used to perform proximate, ultimate, calorific value and TGA analyses.

Physicochemical characterization and thermogravimetric analysis

Physicochemical characterization of biomass samples includes proximate, ultimate and higher heating value analyses. Proximate and ultimate analyses are basic characterization methods for biofuel quality of the biomass sample affecting its calorific value [30].

The proximate analysis was performed by an ash oven (Protech Lab PMF-1103, Turkey) according to the related ASTM standards to determine moisture content, volatile matter and ash content [31]. The fixed carbon of the samples was calculated by the difference between 100 and the sum of the moisture content, volatile matter and ash content.

Ultimate analysis was carried out using an elementary analyzer (LECO CHNS-932, USA) to determine the ultimate percentages of C, H, N and S elements. The oxygen content was calculated by the difference. Higher heating value was determined using a bomb calorimeter (IKA C5000, Germany).

Proximate, ultimate and higher heating value analyses of sour cherry stalk and flesh are summarized in Table 1.

TG (thermogravimetry) and DTG (derivative thermogravimetry) curves are fundamental tools for determination

**Table 1** Ultimate and proximate analysis of sour cherry stalk and flesh

	Sour cherry stalk	Sour cherry flesh
Proximate analysis/%		
Moisture	10	12.20
Ash	2.10	2.80
Volatiles	67.12	67.60
Fixed C*	20.78	17.40
Ultimate analysis/%		
C	43.18	41.21
H	6.32	6.41
O*	49.59	50.71
N	0.91	1.67
S	–	–
Higher heating value/J g^{-1}	16429	15918

*By difference

of thermal characteristics in a pyrolysis process. TG curve implies the mass loss of a sample as a function of temperature or time, DTG curve, on the other side, is the first-order derivative of TG curve from which maximum mass loss rates and their corresponding temperatures can be determined. Thermal decomposition of sour cherry residues was carried out using a thermogravimetric analyzer EXSTAR SII TG/DTA 6300, (Seiko Instruments, Japan). The sieved fractions of 6 mg $\pm$ 0.01 mg of sample were placed in a small alumina crucible for each experiment and heated from ambient temperature to a maximum temperature of 1000 °C. In order to prevent oxidation, an inert nitrogen atmosphere with a flow of 200 mL min^{-1} was used. The change in mass loss was recorded and evaluated. Each experiment was repeated at least two times to ensure repeatability.

Kinetic modeling

Pyrolysis of biomass occurs by a degradation reaction, and during the process, biomass is converted to volatiles and solid residue (char) [6]:

$$\text{Biomass} \rightarrow \text{volatiles} + \text{char} \tag{1}$$
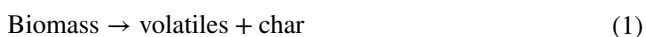
The equation rate of thermal degradation reaction from solid state to volatile product can be expressed as follows [32]:

$$\frac{d\alpha}{dt} = k(T)f(\alpha) \tag{2}$$

where α is the conversion degree, t is the time, k is the reaction constant, T is the temperature, and $f(\alpha)$ is the reaction model related to the solid reaction mechanism. As defined in Eq. (2) the rate of pyrolysis, $\frac{d\alpha}{dt}$, at a constant temperature,

is dependent on the reaction rate, k, and the reaction conversion model $f(\alpha)$.

$k(T)$, the dependency of the rate constant on temperature, is defined by the Arrhenius equation:

$$k(T) = A e^{-\left(\frac{E_a}{RT}\right)} \tag{3}$$

where A is the pre-exponential factor, E_a is the apparent activation energy, T is the absolute temperature, and R is the universal gas constant.

The degree of conversion, α, represents the transformed amount of biomass and can be described as:

$$\alpha = \frac{m_i - m_t}{m_i - m_f} \tag{4}$$

where m_i, m_t, m_f are the initial mass of the biomass sample, the mass of the sample at time t, and the final mass of the biomass sample, respectively.

Combination of Eqs. (2) and (3) gives the general Eq. (5) to calculate the kinetic parameters for isothermal conditions:

$$\frac{d\alpha}{dt} = A e^{-\left(\frac{E_a}{RT}\right)} f(\alpha) \tag{5}$$

However, since isothermal conditions require more time during experiments and non-isothermal procedure could give equivalent information as well as isothermal procedure, non-isothermal conditions are much more preferred. For non-isothermal thermogravimetric experiments, heating rate, $\beta = \frac{dT}{dt}$, can be substituted into Eq. (5) by giving Eq. (6) and used in the differential methods:

$$\frac{d\alpha}{dT} = \frac{A}{\beta} e^{-\left(\frac{E_a}{RT}\right)} f(\alpha) \tag{6}$$

Equation (6) represents the fraction of biomass decomposed in the course of experimental time. The integral form of Eq. (6) can be given as Eq. (7) and used in the integral methods [9, 33]:

$$g(\alpha) = \int_0^\alpha \frac{1}{f(\alpha)} d\alpha = \frac{A}{\beta} \int_0^T e^{-\frac{E_a}{RT}} dT = \frac{A E_a}{\beta R} \int_x^\infty \frac{e^{-x}}{x^2} dx = \frac{A E_a}{\beta R} p(x) \tag{7}$$

where $g(\alpha)$ is the integral form of $f(\alpha)$, x is E_a/RT, and $p(x)$ is the temperature integral. The kinetic parameters can be determined from the general Eqs. (5) and (6) or the integral form of Eq. (7) analytically by means of mathematical models. Since $p(x)$ has no analytical solution, some approximations were given. Assuming that $x = E_a/RT$ is a constant, Doyle [34] suggested:

$$p(x) = \exp(-1,0518x - 5,330) \quad x > 20 \tag{8}$$

Coats and Redfern [35] suggested:

$$p(x) = \frac{\exp(-x)}{x^2}\left(1 - \frac{2}{x}\right) \tag{9}$$

In the present study, TG/DTG data were used to determine the activation energy (E_a) based on isoconversional methods. Model-free methods are more reliable compared with model-fitting methods and lead more accurate calculation of activation energies [36]. Activation energies of sour cherry stalk and flesh were estimated by using isoconversional (model-free) methods. Integral model-free methods including Flynn–Wall–Ozawa (FWO) and Kissinger–Akahira–Sunose (KAS) were applied in addition to Friedman method which is a differential model-free method.

Friedman method

The apparent activation energy (E_a) can be obtained from the slope of the plot of $\ln(\beta d\alpha/dT)$ against $1/T$ at various heating rates for a given conversion value [37]:

$$\ln\left(\beta\frac{d\alpha}{dT}\right) = \ln A + \ln f(\alpha) - \frac{E_a}{RT} \tag{10}$$

Equation (10) can be attained by taking natural logarithms of both sides of the general Eq. (6) at a given α. As a consequence, $f(\alpha)$ remains constant and determination of activation energy requires no assumption about reaction model.

Flynn–Wall–Ozawa (FWO) method

The Flynn–Wall–Ozawa method [38, 39] starts from Eq. (7) and employs Doyle's approximation [34] which was represented by Eq. (8). The FWO method allows the determination of apparent activation energy by Eq. (11):

$$\ln \beta = \ln\frac{AE_a}{Rg(\alpha)} - 5.331 - 1.052\frac{E_a}{RT} \tag{11}$$

The FWO method allows the determination of apparent activation energy from the slope of the linear regression line of $\ln \beta$ versus $1/T$ plot.

Kissinger–Akahira–Sunose (KAS) method

Kissinger–Akahira–Sunose method [40, 41] starts from Eq. (7) as well and employs the Coats–Redfern approximation of $p(x)$ which was represented in Eq. (9) to the equation:

$$\ln\frac{\beta}{T^2} = \ln\left(\frac{AR}{E_a g(\alpha)}\right) - \frac{E_a}{RT} \tag{12}$$

The Kissinger–Akahira–Sunose (KAS) method allows the calculation of apparent activation energy from the slope of the linear line in the plot of $\ln \beta/T^2$ versus $1/T$.

Results and discussion

Physical and chemical characterization

Proximate analysis consists of moisture, ash, volatile matter and fixed carbon determination. As it can be seen from Table 1, the moisture content of sour cherry stalk is slightly lower than sour cherry flesh since fruit fleshes are to be expected to contain relatively higher moisture. High moisture content is undesired since it affects the fuel quality by mainly decreasing its heating value. For this reason, to ensure the energy-efficient operation of the process and to ensure that the fuel has a higher heating value, further pre-drying of sour cherry stalk and flesh samples may be considered. Volatile matter and fixed carbon contents indicate the ignition easiness as an energy source [15]. The results of volatile matter and fixed detectable carbon contents of sour cherry stalk and flesh were within the range of many general biomass [42]. High ash content as being a disadvantage for a possible bioenergy source is related to the reduction in available energy of the fuel [43]. Ash content of sour cherry stalk and flesh exhibited relatively low levels compared with some other biomass samples [44].

Ultimate analysis results of sour cherry stalk and flesh revealed C, H, O, N and S contents. Aside from the comparable results of other common biomass samples [42], no sulfur content leads low greenhouse gas emissions which is an important positive sign for environmental concerns. Furthermore, higher heating value of sour cherry stalk and flesh was 16429 and 15918 J g^{-1}, respectively. Relative moderate levels of moisture content could have an influence on the higher heating value of the sample.

Thermal characteristics

At the scope of the present work, the TG and DTG curves of biomass waste materials, namely flesh and stalk of sour cherry obtained from fruit juice production facility, at five different heating rates (5, 10, 20, 30 and 40 °C min^{-1}) and two different particle sizes (75–150 and 150–250 μm) are given in Fig. 1. The following observations and/or comments can be organized by thoroughly examining the TG/DTG curves (Fig. 1) obtained for sour cherry flesh and sour cherry stalk at 10 °C min^{-1} heating rate and 75–150 μm particle size:

The pyrolysis processes of sour cherry flesh and sour cherry stalk occurred in four different stages in that there exist four main slope changes in TG curves and their corresponding peaks on DTG curves. The stages represented by the highest two peaks on the DTG curves and their corresponding highest inclined stages on the TG curves
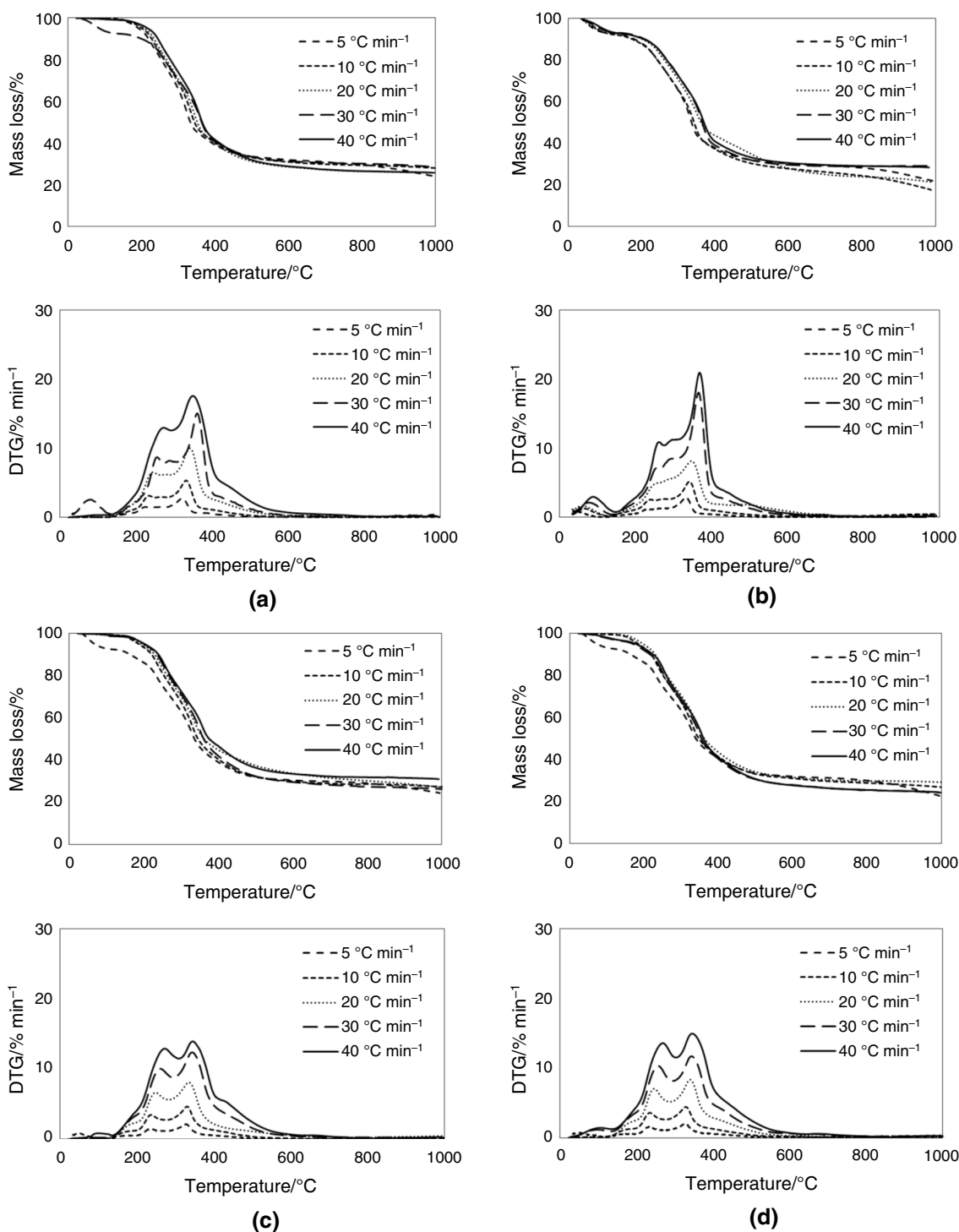
Fig. 1 TG and DTG curves at different heating rates and particle sizes **a** sour cherry stalk (75–150 μm), **b** sour cherry stalk (150–250 μm), **c** sour cherry flesh (75–150) μm, **d** sour cherry flesh (150–250 μm)

(approximately between 190 and 380 °C) are called as active pyrolysis stages since these stages demonstrate the highest mass loss rates during the pyrolysis process. Active pyrolysis stage (or zone) is defined as the temperature range between 180 and 400 °C where the major

devolatilization of biomass takes place [32]. Thus, the temperature range of active pyrolysis stage obtained in the present study is consistent with the literature. As it can be seen from Fig. 1a, the active pyrolysis stage of sour cherry stalk includes a shoulder-shaped peak, whereas the active

pyrolysis stage of sour cherry flesh (Fig. 1c) includes a split peak rather than a shoulder peak.

The first stages (Stage 1) were observed between 25–191 °C and 25–196 °C for sour cherry stalk and sour cherry flesh, respectively. The mass losses of Stage 1 are attained from Fig. 1a, c as 3.9% and 6.1% for sour cherry stalk and sour cherry flesh, respectively. These mass losses were mainly be attributed to the removal of water both present in biomass wastes and bounded to biomass wastes by surface tension. Moreover, some volatile compounds, especially that have low molecular weights, may be removed at the first stage as well.

The second stages (Stage 2) of sour cherry stalk and sour cherry flesh were observed to be between 191–311 °C and 196–305 °C with mass losses of 30.77% and 27.83%, respectively. The corresponding areas on the DTG curves (Fig. 1a, c) were represented by the peaks at 234 °C and 237 °C for sour cherry stalk and sour cherry flesh, respectively. The maximum mass loss rates occurred at these temperatures were designated to be 3.82% min^{-1} and 3.28% min^{-1}. Stage 2 can be entitled as an active pyrolysis stage due to the high mass loss rates occurred. Thermal degradation behaviors of main biomass components such as hemicellulose, cellulose and lignin have been well studied, and hemicellulose is known to decompose at the temperature interval of 150–350 °C [45]. Thus, Stage 2 can be attributed mainly to hemicellulose decomposition.

The third stage (Stage 3) of sour cherry stalk, which was denoted by the peak at 332 °C on DTG curve (Fig. 1a), started at 311 °C and finished at 376 °C with a mass loss of 22.18% at a maximum mass loss rate of 5.23% min^{-1}. Similarly, the third stage of sour cherry flesh occurred from 305 °C to 389 °C, which was demonstrated with the peak at 331 °C on DTG curve (Fig. 1c). The mass loss and maximum mass loss rate for sour cherry flesh were read as 24.45% and 4.49% min^{-1}, respectively. Stage 3, similarly to Stage 2, can also be defined as active pyrolysis stage due to the encountered high mass loss rates. The mass loss rates obtained in Stage 3, both for sour cherry stalk and sour cherry flesh, were the highest mass loss rates during the whole pyrolysis processes as it can clearly be confirmed from DTG curves by examining related peaks. Stage 3 can be attributed mainly to cellulose since cellulose is known to decompose at the temperature range of 270–350 °C [45].

The fourth and the last stages (Stage 4) of pyrolysis process for sour cherry stalk and sour cherry flesh laid down in the temperature ranges of 376–1000 °C and 389–1000 °C with mass losses of 15.25% and 14.74%, respectively. The residual masses at the end of the overall pyrolysis process were determined as 27.96% and 27.08% for sour cherry stalk and sour cherry flesh, respectively. Stage 4 can be referred as passive pyrolysis stage since the mass loss rates obtained at the last stage are much lower compared to those obtained

at Stage 2 and Stage 3. Stage 4 can be attributed mainly to lignin since the temperature range of lignin decomposition is known to be between 160 and 900 °C [3].

Therefore, considering the above information given, active pyrolysis of sour cherry flesh and stalk ends at around 389 °C and 376 °C, with a total mass loss of 58.18% and 56.78%, respectively. Thus, pyrolysis process of these biomass waste materials should be conducted at least at around 375–390 °C pyrolysis temperature in order to obtain 57.5% average pyrolysis conversion based on volatiles which is especially important for the processes targeting liquid products. Further temperature increments are not expected to increase liquid product yields significantly since the increased temperature values would fall into the passive pyrolysis stage which is mainly responsible for char formation.

TG/DTG curves do not enable the exact calculation of hemicellulose, cellulose and lignin ratios of a biomass sample since these components decompose in overlapping temperature ranges, and they do not completely decompose but also form an overall residue. On the other hand, there exist two important information in the literature that we can rely on their usage in rough estimation of these components ratios based on the results given in the present section. The first information is the residue amount yielded by lignin at the end of a pyrolysis process. A literature search [46–50] revealed the arithmetic mean of residue amount yielded by several different lignin samples at the end of pyrolysis as 44% of initial sample by mass. The second information is the structural content of biomass samples. Biomass materials are lignocellulosic materials that consist mainly cellulose, hemicellulose and lignin. Thus, the origins of the residual mass obtained at the end of pyrolysis are mainly hemicellulose, cellulose and lignin. In other words, the origin of the residual mass other than lignin can be assumed as hemicellulose and cellulose, together called as holocellulose. Therefore, combining these two information and the results given in the present section, the holocellulose–lignin ratios of sour cherry stalk and sour cherry flesh were roughly estimated as 69–27% and 68–26%, respectively.

The effect of parameters on characteristics of active pyrolysis stages

The characteristic properties of active pyrolysis stages (Stage 2 and Stage 3), namely starting temperature (T_i), ending temperature (T_f), maximum mass loss rate (W_{max}) and the temperature at which maximum mass loss rate occurred (T_{max}), were carefully determined for five different heating rates (5, 10, 20, 30 and 40 °C min^{-1}) and two different particle sizes (75–150 and 150–250 μm) since active pyrolysis stages were subjected to kinetic calculations. The results of

sour cherry flesh and sour cherry stalk are summarized in Tables 2 and 3, respectively.

The effect of heating rate

The heating rate was definitely effective on the characteristic properties of active pyrolysis stages. Examining Tables 2 and 3, it was clearly noticed that all of the characteristic temperatures (i.e., T_i, T_f, T_{max}) of active pyrolysis stages were shifted to higher values as a result of increasing heating rate for all studied biomass types and particle sizes. The shifting of characteristic temperatures to higher values with increasing heating rate was also observed in previous pyrolysis studies of different biomass samples such as *Prosopis juliflora* fuelwood [32], walnut shell [51], woody parts, sawmill dust [52] carton packaging and cardboard [53]. This situation was expected since biomass particles are heated more gradually at lower heating rates leading to an improved and more effective heat transfer to the inner portions and among the particles [3]. In other words, higher heating rates resulted in less efficient and less effective heat transfer to the inner portions and among the particles of studied biomasses. In addition, Tables 2 and 3 reveal that maximum mass loss rates (W_{max}), as well as T_{max}, of active pyrolysis stages were increased with increasing heating rate for all studied biomass types and particle sizes. Since the amount of energy transferred per unit time to the pyrolysis system increases in order to increase the heating rate, an increase in maximum mass loss rate was evaluated as an expected progress.

The effect of particle size

The particle size did also affect the characteristic properties of active pyrolysis stages. Examining Tables 2 and 3, it was observed that all characteristic temperatures of active pyrolysis stages of sour cherry stalk and sour cherry flesh increased with increment in particle size from 75–150 to 150–250 μm for all studied heating rates. Additionally, a similar trend was observed during the pyrolysis study of empty fruit bunch by thermogravimetric analysis [54]. That may simply be due to the non-uniform heating of biomass samples since increasing particle size favors late heating of inner portions of biomass sample and inner biomass particles which in turn leads to the completion of pyrolysis process at higher temperatures. Changing the particle size demonstrated different trends for W_{max} values accordingly to the biomass sample type, studied stage and heating rate. For instance, at Stage 2, increasing particle size of sour cherry flesh resulted in an increase of W_{max} for all studied heating rates. However, the opposite trend was observed for sour cherry stalk, and the increment in particle size resulted in a decrease of W_{max} values for all studied heating rates. The latter was an expected outcome since increasing the particle

Table 2 Properties of active pyrolysis stages for sour cherry flesh

| Property | 5 | | | | 10 | | | | 20 | | | | 30 | | | | 40 | | | |
| | 2nd stage | | 3rd stage | | 2nd stage | | 3rd stage | | 2nd stage | | 3rd stage | | 2nd stage | | 3rd stage | | 2nd stage | | 3rd stage | |
Heating rate/°C min^{-1}	75–150 μm	150–250 μm	75–150 μm	150–250 μm	75–150 μm	150–250 μm	75–150 μm	150–250 μm	75–150 μm	150–250 μm	75–150 μm	150–250 μm	75–150 μm	150–250 μm	75–150 μm	150–250 μm	75–150 μm	150–250 μm	75–150 μm	150–250 μm
T_i/°C	195	196	295	311	196	196	305	314	198	197	310	328	197	198	329	332	197	200	344	330
T_f/°C	295	311	388	389	305	314	389	393	310	328	392	394	329	332	421	417	344	330	423	435
T_{max}/°C	235	235	325	326	237	238	331	332	246	247	335	340	261	262	342	345	270	272	344	349
W_{max}/% min^{-1}	1.41	1.47	2.10	1.71	3.28	3.47	4.49	4.35	6.41	6.88	7.95	7.87	9.94	10.21	12.62	11.63	12.9	13.49	13.91	14.88

Table 3 Properties of active pyrolysis stages for sour cherry stalk

| Property | 5 | | | | 10 | | | | 20 | | | | 30 | | | | 40 | | | |
| | 2nd stage | | 3rd stage | | 2nd stage | | 3rd stage | | 2nd stage | | 3rd stage | | 2nd stage | | 3rd stage | | 2nd stage | | 3rd stage | |
Heating rate/°C min⁻¹	75–150 µm	150–250 µm	75–150 µm	150–250 µm	75–150 µm	150–250 µm	75–150 µm	150–250 µm	75–150 µm	150–250 µm	75–150 µm	150–250 µm	75–150 µm	150–250 µm	75–150 µm	150–250 µm	75–150 µm	150–250 µm	75–150 µm	150–250 µm
T_i/°C	185	195	302	311	191	197	311	324	196	199	325	323	204	207	333	342	200	210	336	337
T_f/°C	302	311	352	365	311	324	376	381	325	323	387	396	333	342	405	400	336	337	423	419
T_{max}/°C	225	261	321	333	234	272	332	342	245	287	343	346	256	293	362	367	271	296	354	369
W_{max}/% min⁻¹	1.85	1.74	2.75	2.72	3.82	2.64	5.23	5.10	6.52	5.42	9.92	8.06	8.60	8.4	14.98	17.79	12.79	11.25	17.49	20.16

size is thought (1) to lead poor heat transfer to the inner parts causing low average particle temperature and hence low yields of volatiles and (2) to form an extra barrier against the inner-formed volatiles trying to escape from the surface. Increasing the particle size resulted in a decrease in W_{max} values of Stage 3 for sour cherry flesh up to 30 °C min⁻¹ heating rate and for sour cherry stalk up to 20 °C min⁻¹ heating rate. At higher heating rates for Stage 3, W_{max} values of both sour cherry flesh and sour cherry stalk increased by increasing particle size, possibly due to the overcoming of at least some fraction of mass and/or heat transfer limitations.

The residual mass amounts of sour cherry stalk with a particle size of 75–150 µm at the end of pyrolysis process were determined at 5, 10, 20, 30 and 40 °C min⁻¹ as 23.86%, 27.96%, 25.57%, 28.54% and 25.60%, whereas the residual mass amounts of sour cherry flesh with the same particle size were determined as 24.38%, 27.08%, 26.89%, 26.07% and 30.91%, respectively. Correspondingly, the residual mass amounts of sour cherry stalk with a particle size of 150–250 µm at the end of pyrolysis process were determined at 5, 10, 20, 30 and 40 °C min⁻¹ as 21.7%, 17.42%, 21.02%, 28.85% and 28.25%, whereas the residual amounts of sour cherry flesh with the same particle size were determined as 22.57%, 26.78%, 29.29%, 24.29% and 24.40%, respectively.

Kinetic analysis

Thermogravimetric decomposition of the biomass samples was investigated by dividing analysis graphics into four stages, and kinetic analysis of each active stage was separately determined.

Using the experimental temperature data in Tables 2 and 3, the activation energies of both biomass types were calculated by application of Friedman method, which was given in Eq. 10, from the slope of the curve found as a result of regression analysis of $1/T$ versus $\ln\beta(d\alpha/dT)$ plot, at certain conversion degrees. Likewise, the activation energy of the samples at certain conversion degrees was calculated from the slope of the curve obtained by regression analysis of $1/T$ versus $\ln\beta$ plot and $1/T$ versus $\ln\beta/T^2$ plot by applying FWO method and KAS method given in Eqs. 11 and 12, respectively.

For Friedman, FWO and KAS methods, plots of sour cherry stalk samples with a particle size of 75–150 µm at the second active stage and the third active stage are demonstrated in Figs. 2 and 3, respectively. Calculated R^2 values, activation energies and obtained fitted equations of sour cherry stalk samples with a particle size of 75–150 µm are presented in Tables 4 and 5 at the second active stage and the third active stage, respectively. The results reveal that average activation energies of sour cherry stalk samples at the second active stage were 160.5, 159.7 and 159.0 kJ mol⁻¹ for Friedman, FWO and KAS methods, respectively, whereas
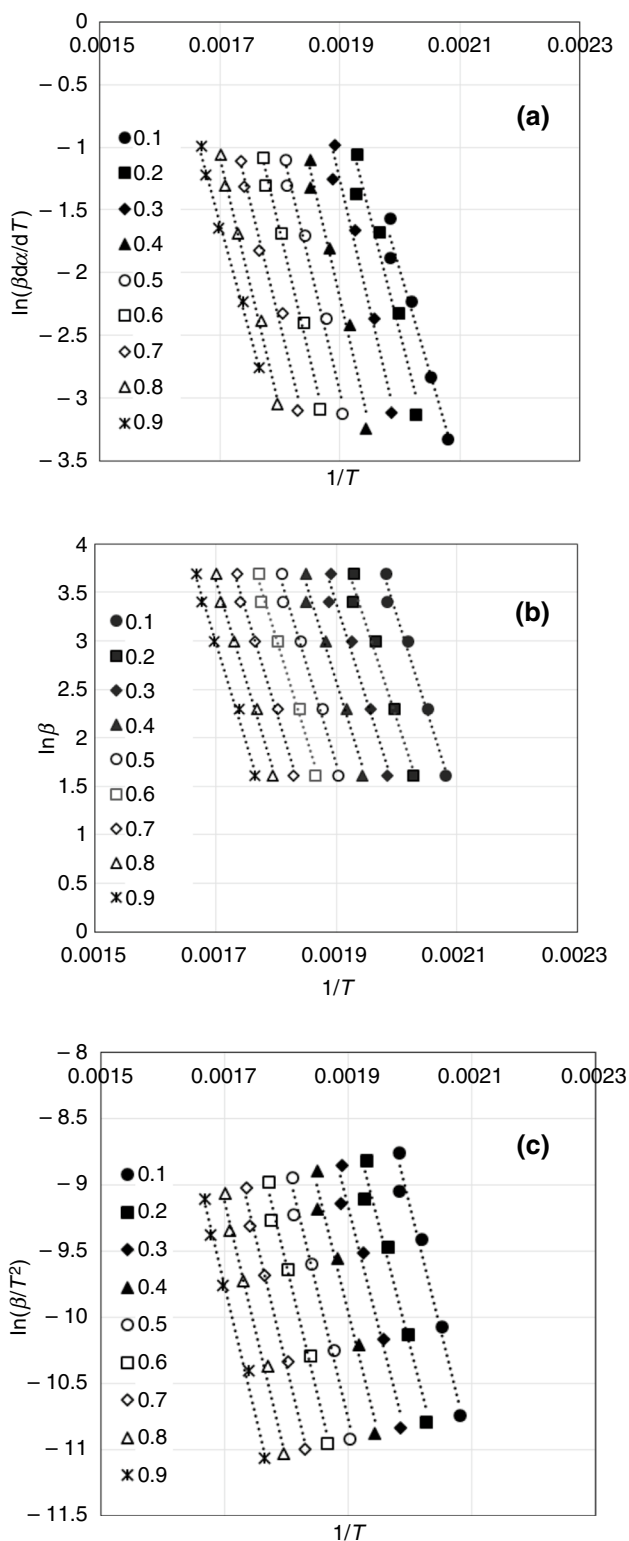
Fig. 2 Isoconversional plots of sour cherry stalk with a particle size of 75–150 μm at the second active stage **a** Friedman, **b** FWO, **c** KAS method
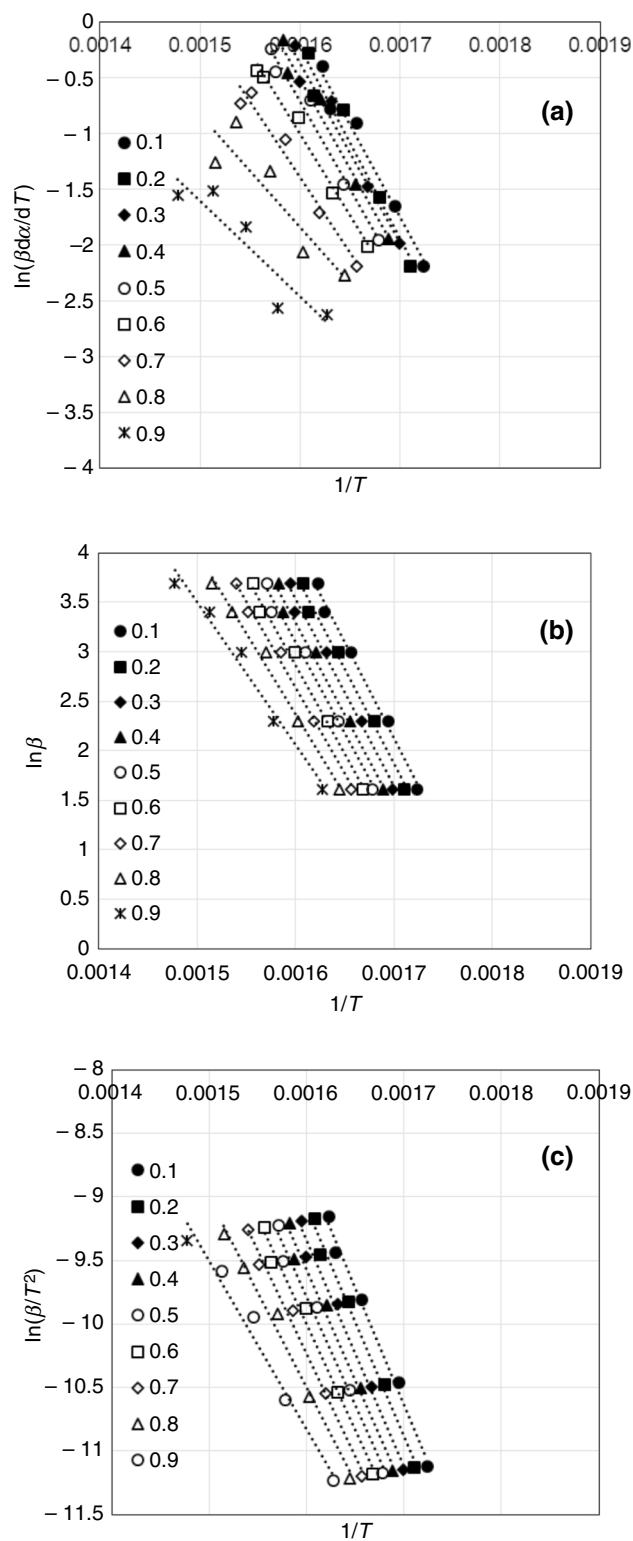
Fig. 3 Isoconversional plots of sour cherry stalk with a particle size of 75–150 μm at the third active stage **a** Friedman, **b** FWO, **c** KAS method

Table 4 Fitted equations, calculated activation energies and the coefficients of determination using Friedman, FWO and KAS methods for the sour cherry stalk with a particle size of 75–150 µm at the second active stage

α	Friedman			FWO			KAS		
	Fitted equation	R^2	E_a	Fitted equation	R^2	E_a	Fitted equation	R^2	E_a
0.1	$y=-16499x+31.021$	0.9744	137.2	$y=-19622x+42.509$	0.9789	155.1	$y=-18637x+28.108$	0.9766	154.9
0.2	$y=-18696x+34.908$	0.9545	155.4	$y=-19253x+40.717$	0.9732	152.2	$y=-18240x+26.262$	0.9702	151.6
0.3	$y=-20242x+37.182$	0.97	168.3	$y=-19739x+40.887$	0.97	156.0	$y=-18705x+26.391$	0.9666	155.5
0.4	$y=-20898x+37.493$	0.9764	173.7	$y=-20265x+41.074$	0.9771	160.2	$y=-19208x+26.535$	0.9745	159.7
0.5	$y=-20073x+35.188$	0.9817	166.9	$y=-20492x+40.683$	0.9822	161.9	$y=-19413x+26.102$	0.9801	161.4
0.6	$y=-20205x+34.691$	0.9871	168.0	$y=-20608x+40.131$	0.9849	162.9	$y=-19507x+25.510$	0.9831	162.2
0.7	$y=-19485x+32.654$	0.9802	162.0	$y=-20632x+39.422$	0.9899	163.1	$y=-19509x+24.760$	0.9887	162.2
0.8	$y=-20004x+32.921$	0.9935	166.3	$y=-20712x+38.851$	0.9918	163.7	$y=-19567x+24.151$	0.9908	162.7
0.9	$y=-17686x+28.465$	0.9936	147.0	$y=-20552x+37.931$	0.9919	162.4	$y=-19386x+23.195$	0.9909	161.2

Table 5 Fitted equations, calculated activation energies and the coefficients of determination using Friedman, FWO and KAS methods for the sour cherry stalk with a particle size of 75–150 µm at the third active stage

α	Friedman			FWO			KAS		
	Fitted equation	R^2	E_a	Fitted equation	R^2	E_a	Fitted equation	R^2	E_a
0.1	$y=-16533x+26.347$	0.9735	137.5	$y=-19541x+35.344$	0.9929	154.4	$y=-18345x+20.555$	0.9919	152.5
0.2	$y=-17262x+27.399$	0.9636	143.5	$y=-19171x+34.453$	0.9906	151.5	$y=-17964x+19.647$	0.9893	149.4
0.3	$y=-16086x+25.371$	0.9701	133.7	$y=-18859x+33.700$	0.989	149.0	$y=-17643x+18.879$	0.9874	146.7
0.4	$y=-16153x+25.333$	0.9737	134.3	$y=-18616x+33.086$	0.988	147.1	$y=-17391x+18.251$	0.9862	144.6
0.5	$y=-15683x+24.376$	0.977	130.4	$y=-18408x+32.544$	0.9874	145.5	$y=-17175x+17.695$	0.9855	142.8
0.6	$y=-14542x+22.254$	0.9866	120.9	$y=-17954x+31.598$	0.9892	141.9	$y=-16712x+16.734$	0.9874	138.9
0.7	$y=-13661x+20.462$	0.9674	113.6	$y=-17445x+30.549$	0.9927	137.9	$y=-16192x+15.669$	0.9915	134.6
0.8	$y=-10080x+14.293$	0.8167	83.8	$y=-16270x+28.402$	0.9915	128.6	$y=-15003x+13.499$	0.9899	124.7
0.9	$y=-8615.6x+11.318$	0.8493	71.6	$y=-14465x+25.195$	0.979	114.3	$y=-13176x+10.257$	0.9744	109.5

at the third stage were 118.8, 141.1 and 138.2 kJ mol^{-1}. As given above, the average activation energies at the third active stage were lower than the average activation energies at the second active stage. The end result could be explained by the indication that cellulose mainly starts to be decomposed in the second active stage. Since higher thermal decomposition characteristics of the cellulose need more energy to be decomposed [55], the average activation energies of the second stage were relatively higher than the third active stage. Additionally, the average activation energies of sour cherry stalk biomass samples obtained by all the three applied methods remained moderately close to each other for both active stages.

Plots of estimation of activation energies of sour cherry stalk with a particle size of 150–250 µm for Friedman, FWO and KAS methods are given in Figs. 4 and 5, for the second and the third active stage, respectively. Activation energies of sour cherry stalk with a particle size of 150–250 µm, which were attained through the related plots for a given value of conversion degree from 0.1 to 0.9, are given in Tables 6 and 7 for all studied model-free methods. The

activation energy was observed to be a function of conversion degree due to the multistep reaction mechanism. The average activation energies of sour cherry stalk with a particle size of 150–250 µm calculated from Friedman, FWO and KAS methods at the second active stage were 179.7, 179.8 and 180.0 kJ mol^{-1}, while at the third stage were 162.1, 164.6 and 162.7 kJ mol^{-1}, respectively. The estimated activation energy values correlate sufficiently for all the applied methods. The average activation energies of sour cherry stalk at the higher particle size were higher at the second active stage than at the third active stage. The similar tendency could additionally be seen for the lower particle size about the fact that the average activation energies were higher at the second active stage in comparison with the third active stage. Moreover, higher particle size of sour cherry stalk gave relatively higher average activation energies compared with the lower particle size at both active stages. The reason for that could be the heat transfer limitation between particles. When the particle size increases, the heat transfer between particles decreases and as a result less particles come in contact; hence, reaction possibility
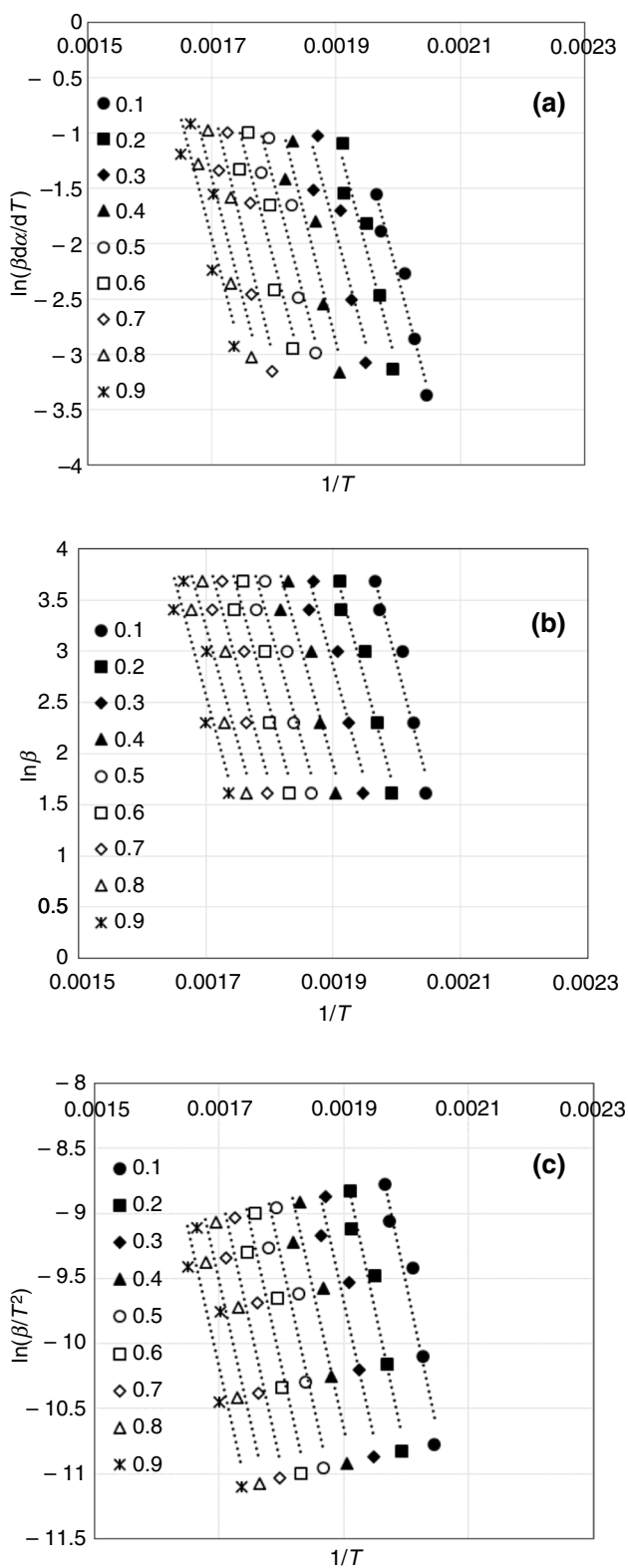
Fig. 4 Isoconversional plots of sour cherry stalk with a particle size of 150–250 μm at the second active stage **a** Friedman, **b** FWO, **c** KAS method
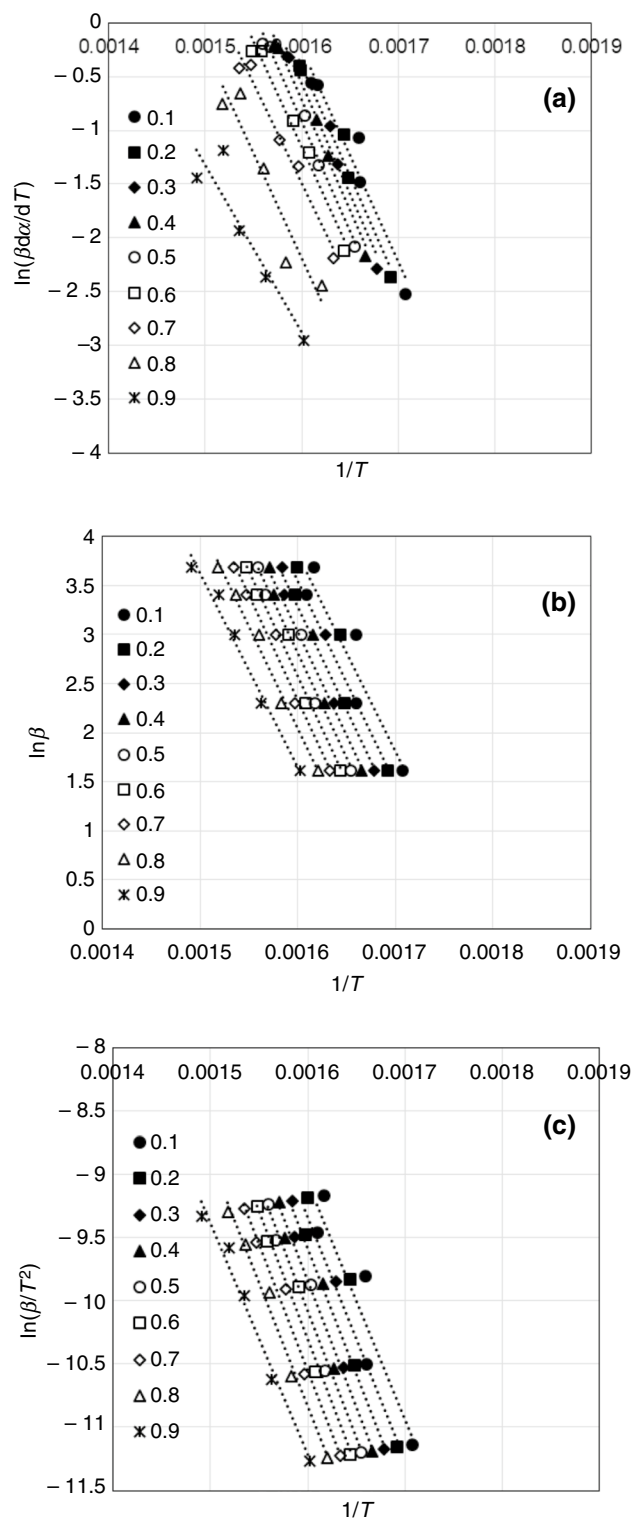
Fig. 5 Isoconversional plots of sour cherry stalk with a particle size of 150–250 μm at the third active stage **a** Friedman, **b** FWO, **c** KAS method

Table 6 Fitted equations, calculated activation energies and the coefficients of determination using Friedman, FWO and KAS methods for the sour cherry stalk with a particle size of 150–250 µm at the second active stage

α	Friedman			FWO			KAS		
	Fitted equation	R^2	E_a	Fitted equation	R^2	E_a	Fitted equation	R^2	E_a
0.1	$y=-20878x+39.450$	0.9552	173.6	$y=-23825x+50.540$	0.9374	188.3	$y=-22826x+36.114$	0.9321	189.8
0.2	$y=-21530x+39.903$	0.9279	179.0	$y=-23066x+47.701$	0.9525	182.3	$y=-22039x+33.219$	0.9482	183.2
0.3	$y=-20983x+37.957$	0.8567	174.5	$y=-22484x+45.572$	0.9172	177.7	$y=-21433x+31.042$	0.9095	178.2
0.4	$y=-22327x+39.522$	0.8762	185.6	$y=-22359x+44.379$	0.888	176.7	$y=-21283x+29.803$	0.8776	176.9
0.5	$y=-21133x+36.576$	0.852	175.7	$y=-22500x+43.767$	0.8838	177.8	$y=-21402x+29.150$	0.873	177.9
0.6	$y=-21020x+35.664$	0.8324	174.8	$y=-22647x+43.234$	0.8644	179.0	$y=-21527x+28.577$	0.8519	179.0
0.7	$y=-23119x+38.578$	0.8036	192.2	$y=-22771x+42.679$	0.8435	180.0	$y=-21629x+27.985$	0.8292	179.8
0.8	$y=-21883x+35.778$	0.7892	181.9	$y=-22562x+41.587$	0.8192	178.3	$y=-21399x+26.856$	0.8028	177.9
0.9	$y=-21650x+34.830$	0.809	180.0	$y=-22506x+40.841$	0.8178	177.9	$y=-21323x+26.076$	0.801	177.3

Table 7 Fitted equations, calculated activation energies and the coefficients of determination using Friedman, FWO and KAS methods for the sour cherry stalk with a particle size of 150–250 µm at the third active stage

α	Friedman			FWO			KAS		
	Fitted equation	R^2	E_a	Fitted equation	R^2	E_a	Fitted equation	R^2	E_a
0.1	$y=-19958x+31.703$	0.9391	165.9	$y=-20075x+35.937$	0.8868	158.7	$y=-18868x+21.131$	0.8736	156.9
0.2	$y=-20406x+32.248$	0.9708	169.7	$y=-20564x+36.442$	0.9144	162.5	$y=-19345x+21.617$	0.9043	160.8
0.3	$y=-20735x+32.614$	0.9774	172.4	$y=-20928x+36.764$	0.9368	165.4	$y=-19699x+21.923$	0.9292	163.8
0.4	$y=-20624x+32.281$	0.9857	171.5	$y=-21133x+36.850$	0.9531	167.0	$y=-19895x+21.993$	0.9473	165.4
0.5	$y=-20366x+31.656$	0.9879	169.3	$y=-21328x+36.933$	0.9652	168.6	$y=-20082x+22.064$	0.9609	167.0
0.6	$y=-19663x+30.305$	0.9814	163.5	$y=-21484x+36.951$	0.9764	169.8	$y=-20229x+22.068$	0.9734	168.2
0.7	$y=-18651x+28.345$	0.9765	155.1	$y=-21309x+36.423$	0.9842	168.4	$y=-20045x+21.525$	0.9821	166.7
0.8	$y=-19434x+28.905$	0.8985	161.6	$y=-20864x+35.427$	0.9887	164.9	$y=-19590x+20.512$	0.9872	162.9
0.9	$y=-15645x+22.145$	0.8702	130.1	$y=-19718x+33.204$	0.983	155.8	$y=-18425x+18.261$	0.9805	153.2

decreases, and eventually, the average activation energy needs to be higher in order to overcome the limitations.

In the second part of the studies, sour cherry flesh obtained after squeezing process was analyzed in terms of thermogravimetric aspect. In Figs. 6 and 7, the isoconversional plots of sour cherry flesh with a particle size of 75–150 µm are presented at the second and the third active stage, respectively. Based on the fitted equations, activation energies were calculated and are given in Tables 8 and 9 together with fitted equations and correlation coefficients. The average activation energies of sour cherry flesh with a particle size of 75–150 µm calculated from Friedman, FWO and KAS methods were 136.2, 160.5 and 159.9 kJ/mol at the second active stage and 151.2, 137.0 and 133.7 kJ mol^{-1} at the third active stage, respectively. The results of sour cherry flesh with a particle size of 75–150 µm at the third active stage revealed again lower average activation energies compared with the second stage for FWO and KAS methods, however, not for Friedman method.

Isoconversional plots of sour cherry flesh with a particle size of 150–250 µm are given in Figs. 8 and 9 at the second and the third stage, respectively. The related plots led the calculation of average activation energies which are presented in Tables 10 and 11. The average activation energies of sour cherry flesh with a particle size of 150–250 µm calculated from Friedman, FWO and KAS methods were 266.1, 273.9 and 279.2 kJ mol^{-1} at the second active stage and 179.8, 197.8 and 197.6 kJ mol^{-1} at the third active stage, respectively. The average activation energies of sour cherry flesh with a particle size of 150–250 µm maintained the decreasing trend from the second active stage to the third active stage. The result approves the idea that the cellulose starts to decompose in the second stage causing an increase in energy need and therefore relatively higher activation energy values in comparison with the third stage. In addition to the mentioned fact, higher particle size range of sour cherry flesh delivered higher average activation energy values at both active stages as stated for sour cherry stalk. This consequence emphasizes the heat transfer limitation between particles when particle size increases. On the other hand, both biomass types exhibited quite approximate average activation energy values for all the studied methods.
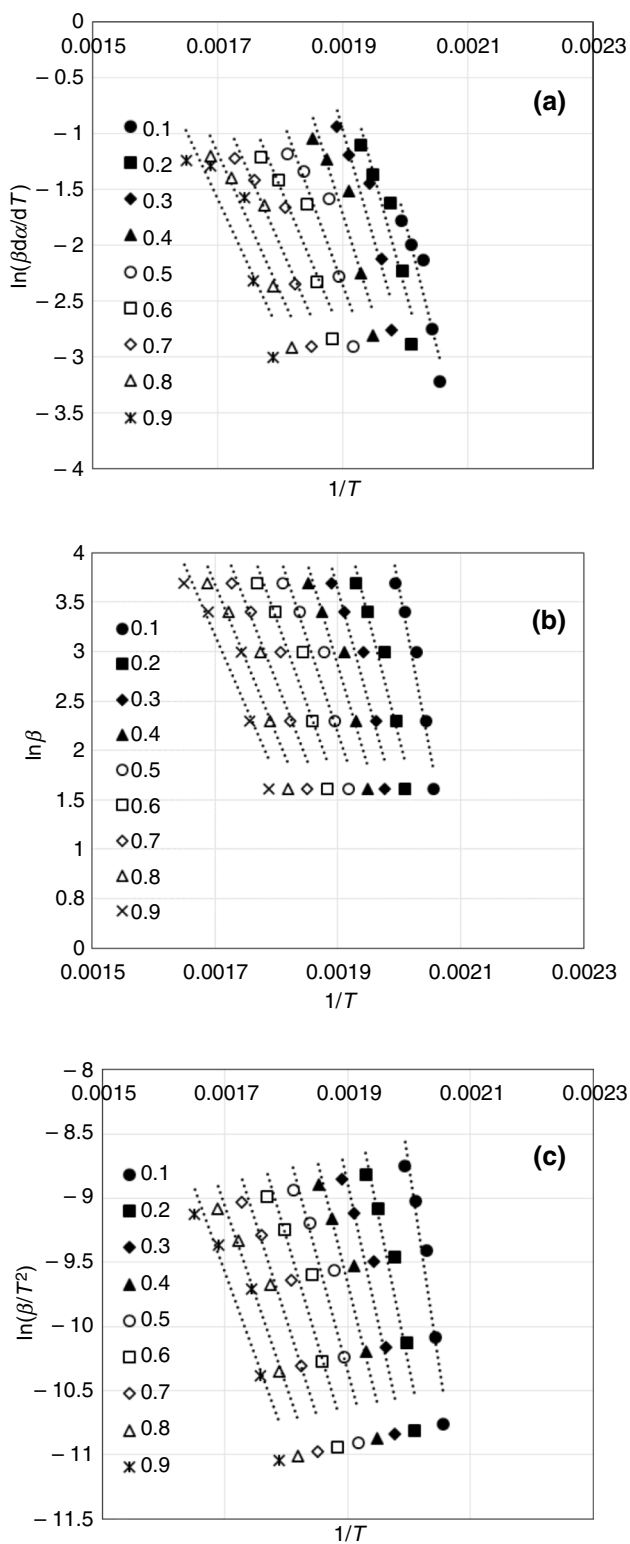
Fig. 6 Isoconversional plots of sour cherry flesh with a particle size of 75–150 μm at the second active stage **a** Friedman, **b** FWO, **c** KAS method
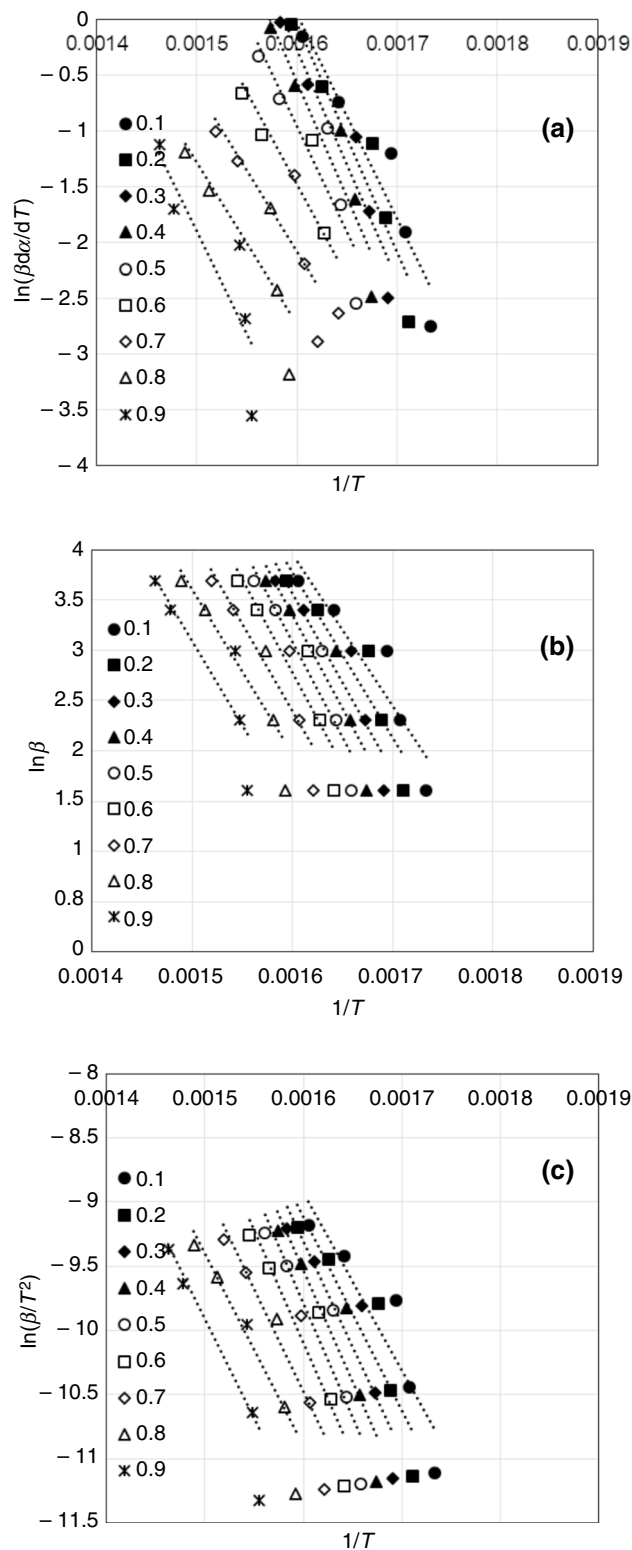

Fig. 7 Isoconversional plots of sour cherry flesh with a particle size of 75–150 μm at the third active stage **a** Friedman, **b** FWO, **c** KAS method

Table 8 Fitted equations, calculated activation energies and the coefficients of determination using Friedman, FWO and KAS methods for the sour cherry flesh with a particle size of 75–150 μm at the second active stage

α	Friedman			FWO			KAS		
	Fitted equation	R^2	E_a	Fitted equation	R^2	E_a	Fitted equation	R^2	E_a
0.1	$y = -22541x + 43.294$	0.9043	187.4	$y = -32764x + 69.177$	0.9433	258.9	$y = -31775x + 54.772$	0.9398	264.2
0.2	$y = -20591x + 38.759$	0.905	171.2	$y = -24681x + 51.467$	0.9314	195.1	$y = -23665x + 37.006$	0.9257	196.8
0.3	$y = -19631x + 36.325$	0.8975	163.2	$y = -22740x + 46.833$	0.9277	179.7	$y = -21705x + 32.336$	0.9211	180.5
0.4	$y = -17858x + 32.214$	0.8901	148.5	$y = -20729x + 42.246$	0.9235	163.8	$y = -19676x + 27.713$	0.9156	163.6
0.5	$y = -15543x + 27.170$	0.852	129.2	$y = -18849x + 38.000$	0.9132	149.0	$y = -17776x + 23.428$	0.9032	147.8
0.6	$y = -13524x + 22.869$	0.8604	112.4	$y = -17319x + 34.500$	0.906	136.9	$y = -16223x + 19.887$	0.894	134.9
0.7	$y = -12995x + 21.398$	0.8559	108.0	$y = -16069x + 31.620$	0.9001	127.0	$y = -14950x + 16.965$	0.886	124.3
0.8	$y = -12596x + 20.244$	0.8482	104.7	$y = -15202x + 29.530$	0.8961	120.1	$y = -14060x + 14.834$	0.8802	116.9
0.9	$y = -12167x + 19.109$	0.7835	101.2	$y = -14375x + 27.600$	0.8868	113.6	$y = -13210x + 12.865$	0.8682	109.8

Table 9 Fitted equations, calculated activation energies and the coefficients of determination using Friedman, FWO and KAS methods for the sour cherry flesh with a particle size of 75–150 μm at the third active stage

α	Friedman			FWO			KAS		
	Fitted equation	R^2	E_a	Fitted equation	R^2	E_a	Fitted equation	R^2	E_a
0.1	$y = -18481x + 29.635$	0.9129	153.7	$y = -15135x + 28.173$	0.8737	119.6	$y = -13936x + 13.379$	0.8539	115.9
0.2	$y = -20512x + 32.781$	0.9047	170.5	$y = -16371x + 29.960$	0.8704	129.4	$y = -15160x + 15.146$	0.8517	126.0
0.3	$y = -20606x + 32.692$	0.912	171.3	$y = -17608x + 31.739$	0.8685	139.2	$y = -16385x + 16.907$	0.8509	136.2
0.4	$y = -20744x + 32.647$	0.8834	172.5	$y = -18641x + 33.171$	0.8705	147.3	$y = -17408x + 18.323$	0.854	144.7
0.5	$y = -18998x + 29.442$	0.8149	157.9	$y = -18990x + 33.470$	0.8652	150.1	$y = -17746x + 18.605$	0.8484	147.5
0.6	$y = -16536x + 24.974$	0.7415	137.5	$y = -18747x + 32.776$	0.8544	148.2	$y = -17491x + 17.890$	0.836	145.4
0.7	$y = -14763x + 21.534$	0.7148	122.7	$y = -17274x + 30.042$	0.8241	136.5	$y = -15999x + 15.126$	0.8005	133.0
0.8	$y = -14583x + 20.596$	0.7044	121.2	$y = -16370x + 28.166$	0.7921	129.4	$y = -15071x + 13.213$	0.7633	125.3
0.9	$y = -18425x + 25.743$	0.7397	153.2	$y = -16863x + 28.386$	0.7556	133.3	$y = -15537x + 13.393$	0.724	129.2

However, the difference in the calculated values for various applied methods was slightly higher when sour cherry flesh was used as biomass type compared to sour cherry stalk. Particularly, the average activation energy values of FWO and KAS methods were quite close to each other for both active stages, when sour cherry flesh and sour cherry stalk were used. Conversely, the Friedman method gave slightly different results than those of two methods for sour cherry flesh, on the contrary not for sour cherry stalk in general. The reason for the varying result can be explained by the fact that the FWO and KAS methods are integral methods giving more accurate results, whereas the Friedman method is a differential method which is vulnerable to experimental noises. The similarity in the results of FWO and KAS methods for other biomass types also was seen in other studies [56, 57]. Although the Friedman method is a differential method, it delivered consistent results for the sour cherry stalk compared with the other two methods.

In terms of particle size, the activation energy values of sour cherry stalk and flesh at 75–150 μm particle size were observed to be close for both active pyrolysis stages by considering the arithmetic average of activation energies calculated from Friedman, FWO and KAS methods. However, for 150–250 μm particle size, the activation energies of sour cherry flesh calculated by taking the arithmetic average of Friedman, FWO and KAS methods' results were higher than those of sour cherry stalk for both active stages, but especially for second stage. Activation energy discloses the minimum amount of energy required for a reaction to be started. Thus, a reaction having high activation energy value starts more difficult than a reaction having low activation energy value. From this point of view, the pyrolysis process of sour cherry flesh is more difficult to proceed than the pyrolysis process of sour cherry stalk for the particle size of 150–250 μm. However, the same comment cannot be made for the particle size of 75–150 μm since the average activation energies of sour cherry flesh and stalk at 75–150 μm particle size were close to each other. Therefore, this inference emphasizes the effect of particle size on the reaction kinetics.
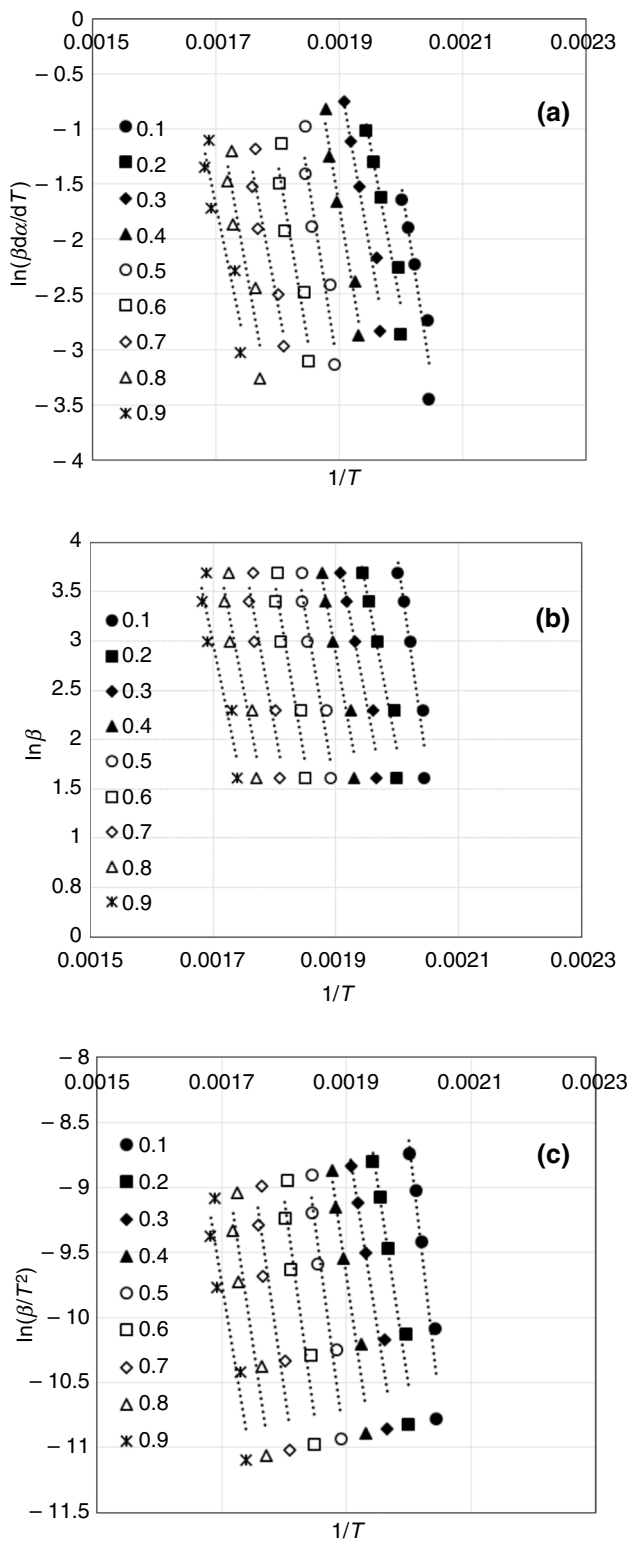
Fig. 8 Isoconversional plots of sour cherry flesh with a particle size of 150–250 μm at the second active stage **a** Friedman, **b** FWO, **c** KAS method
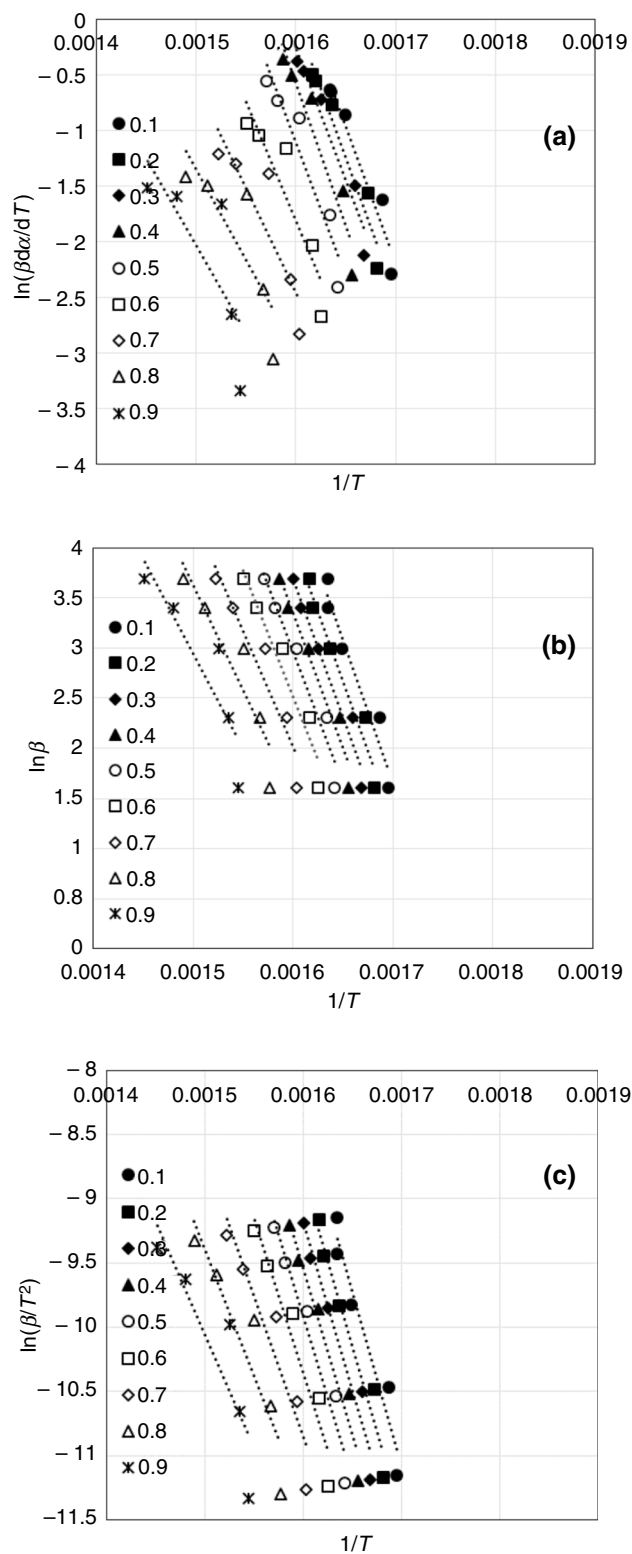
Fig. 9 Isoconversional plots of sour cherry flesh with a particle size of 150–250 μm at the third active stage **a** Friedman, **b** FWO, **c** KAS method

Table 10 Fitted equations, calculated activation energies and the coefficients of determination using Friedman, FWO and KAS methods for the sour cherry flesh with a particle size of 150–250 μm at the second active stage

α	Friedman			FWO			KAS		
	Fitted equation	R^2	E_a	Fitted equation	R^2	E_a	Fitted equation	R^2	E_a
0.1	$y = -36108x + 70.679$	0.904	300.2	$y = -42935x + 89.684$	0.9357	339.3	$y = -41947x + 75.279$	0.9329	348.7
0.2	$y = -29135x + 55.634$	0.9433	242.2	$y = -32816x + 67.497$	0.9423	259.3	$y = -31801x + 53.040$	0.9388	264.4
0.3	$y = -31762x + 59.830$	0.9495	264.1	$y = -32033x + 64.830$	0.9446	253.2	$y = -31001x + 50.337$	0.9411	257.7
0.4	$y = -33908x + 62.695$	0.9701	281.9	$y = -33999x + 67.462$	0.9543	268.7	$y = -32949x + 52.934$	0.9515	273.9
0.5	$y = -36045x + 65.203$	0.9	299.7	$y = -36671x + 71.129$	0.9424	289.8	$y = -35599x + 56.562$	0.9391	296.0
0.6	$y = -33310x + 58.652$	0.8814	276.9	$y = -36387x + 69.083$	0.9157	287.6	$y = -35291x + 54.471$	0.9109	293.4
0.7	$y = -29060x + 49.705$	0.8698	241.6	$y = -34315x + 63.868$	0.8896	271.2	$y = -33193x + 49.210$	0.8829	276.0
0.8	$y = -31182x + 52.229$	0.8587	259.2	$y = -32444x + 59.270$	0.8859	256.4	$y = -31298x + 44.568$	0.8784	260.2
0.9	$y = -27575x + 45.160$	0.8758	229.3	$y = -30306x + 54.513$	0.8916	239.5	$y = -29137x + 39.772$	0.8837	242.2

Table 11 Fitted equations, calculated activation energies and the coefficients of determination using Friedman, FWO and KAS methods for the sour cherry flesh with a particle size of 150–250 μm at the third active stage

α	Friedman			FWO			KAS		
	Fitted equation	R^2	E_a	Fitted equation	R^2	E_a	Fitted equation	R^2	E_a
0.1	$y = -24292x + 39.116$	0.9433	202.0	$y = -28324x + 49.818$	0.9449	223.8	$y = -27122x + 35.021$	0.9402	225.5
0.2	$y = -24627x + 39.394$	0.9411	204.7	$y = -27653x + 48.295$	0.9572	218.5	$y = -26439x + 33.479$	0.9534	219.8
0.3	$y = -23986x + 38.120$	0.9457	199.4	$y = -27282x + 47.333$	0.9615	215.6	$y = -26059x + 32.500$	0.9579	216.7
0.4	$y = -25593x + 40.374$	0.9166	212.8	$y = -27002x + 46.537$	0.9596	213.4	$y = -25769x + 31.688$	0.9557	214.2
0.5	$y = -24086x + 37.423$	0.9059	200.3	$y = -26446x + 45.280$	0.9533	209.0	$y = -25201x + 30.412$	0.9487	209.5
0.6	$y = -21475x + 32.553$	0.8467	178.5	$y = -25321x + 43.032$	0.9385	200.1	$y = -24062x + 28.141$	0.9323	200.1
0.7	$y = -18712x + 27.496$	0.7947	155.6	$y = -23150x + 39.057$	0.9088	183.0	$y = -21870x + 24.134$	0.8988	181.8
0.8	$y = -16206x + 22.952$	0.7	134.7	$y = -21111x + 35.290$	0.8652	166.8	$y = -19806x + 20.328$	0.8494	164.7
0.9	$y = -15679x + 21.488$	0.6	130.4	$y = -18943x + 31.356$	0.8004	149.7	$y = -17608x + 16.348$	0.7758	146.4

Conclusions

Decomposition reaction kinetics of sour cherry stalk and sour cherry flesh was investigated by thermogravimetric analysis. Average activation energies were determined for two different particle size ranges using various model-free methods. According to the obtained TG and DTG data, thermal decomposition of both biomass samples involved multiple stages.

Since the results of average activation energies for the different methods applied were in good agreement, the results could be summarized by taking the average of calculated average activation energies which were obtained by application of Friedman, FWO and KAS methods. Application of various isoconversional methods for different particle size ranges demonstrated that the average activation energy of sour cherry stalk with a particle size of 75–150 μm was at the second active stage 159.8 kJ mol^{-1}, while at the third active stage was 132.7 kJ mol^{-1}. Besides the results of lower particle size, the average activation energies of sour cherry stalk with a particle size of 150–250 μm were 179.8 and 163.1 kJ mol^{-1} for the second and the third active stage, respectively. On the other hand, the average activation energy of sour cherry flesh with a particle size of 75–150 μm was calculated at the second active stage as 152.2 kJ mol^{-1}, while at the third active stage was calculated as 140.6 kJ mol^{-1}. In addition, the average activation energies of sour cherry stalk with a particle size of 150–250 μm were determined 273.1 and 191.7 kJ mol^{-1} at the second and the third active stage, respectively. The higher particle size ranges resulted in relatively higher average activation energies arising from the heat transfer limitation between particles. Moreover, the average activation energies of both biomass samples demonstrated generally lower values at the third active stage in comparison with the second active stage, which is a sign of that the decomposition of cellulose started in the second active region. Comparing the average activation energies calculated by taking the arithmetic average of Friedman, FWO and KAS results, the pyrolysis process of sour cherry flesh at 150–250 μm particle size was found

to proceed more difficult than the pyrolysis process of sour cherry stalk at 150–250 μm particle size. Conversely, the average activation energy values of sour cherry stalk and flesh, calculated by taking the results of arithmetic average of all methods, were fairly close to each other for the 75–150 μm particle size.

In addition, the pyrolysis processes targeting liquid products from sour cherry stalk and flesh should operate at least at pyrolysis temperatures around 375–390 °C to provide 57.5% average pyrolysis conversion based on volatiles.

Experimental results indicate the importance of the effect of particle size of the biomass samples during pyrolysis process as well as the compatibility with the applied model-free methods. Consequently, sour cherry stalk and flesh, which are each residue in juice production, could be evaluated as sustainable feedstock for energy production.

Compliance with ethical standards

Conflict of interest The authors declare that they have no conflict of interest.

References

1. Wu K, Liu J, Wu Y, et al. Pyrolysis characteristics and kinetics of aquatic biomass using thermogravimetric analyzer. Bioresour Technol. 2014;163:18–25.
2. Fu S, Chen H, Yang J, et al. Kinetics of thermal pyrolysis of Eucalyptus bark by using thermogravimetric-Fourier transform infrared spectrometry technique. J Therm Anal Calorim. 2020;139:3527–35.
3. Açıkalın K. Pyrolytic characteristics and kinetics of pistachio shell by thermogravimetric analysis. J Therm Anal Calorim. 2012;109:227–35.
4. Shah MA, Khan MNS, Kumar V. Biomass residue characterization for their potential application as biofuels. J Therm Anal Calorim. 2018;134:2137–45.
5. Ghosh SK. Biomass & bio-waste supply chain sustainability for bio-energy and bio-fuel production. Procedia Environ Sci. 2016;31:31–9.
6. Sharma A, Pareek V, Zhang D. Biomass pyrolysis: a review of modelling, process parameters and catalytic studies. Renew Sust Energy Rev. 2015;50:1081–96.
7. Açıkalın K, Karaca F. Fixed-bed pyrolysis of walnut shell: parameter effects on yields and characterization of products. J Anal Appl Pyrolysis. 2017;125:234–42.
8. Hu Z, Chen Z, Li G, et al. Characteristics and kinetic studies of *Hydrilla verticillata* pyrolysis via thermogravimetric analysis. Bioresour Technol. 2015;194:364–72.
9. Soria-Verdugo A, Goos E, García-Hernando N, et al. Analysis the pyrolysis kinetics of several microalgae species by various differential and integral isoconversional kinetic methods and Distributed Activation Energy Model. Algal Res. 2018;32:11–29.
10. Demirbaş A. Pyrolysis mechanisms of biomass materials. Energ Source Part A. 2009;31(13):1186–93.
11. Di Blasi C. Modelling chemical and physical processes of wood and biomass pyrolysis. Prog Energy Combust Sci. 2008;34:47–90.
12. Vimalathithan PK, Barile C, Vijayakumar CT. Investigation of kinetic triplets for thermal degradation of thermally cured vinyl ester resin systems and lifetime predictions. J Therm Anal Calorim. 2018;133:881–91.
13. Hu M, Chen Z, Wang S, et al. Thermogravimetric kinetics of lignocellulosic biomass slow pyrolysis using distributed activation energy model, Fraser-Suzuki deconvolution and iso-conversional method. Energy Convers Manage. 2016;118:1–11.
14. He Y, Chang C, Li P, et al. Thermal decomposition and kinetics of coal and fermented cornstalk using thermogravimetric analysis. Bioresour Technol. 2018;259:294–303.
15. Das P, Mondal D, Maiti S. Thermochemical conversion pathways of *Kappaphycus alvarezii* granules through study of kinetic models. Bioresour Technol. 2017;234:233–42.
16. Chen D, Shuang E, Liu L. Analysis of pyrolysis characteristics and kinetics of sweet sorghum bagasse and cotton stalk. J Therm Anal Calorim. 2018;131:1899–909.
17. Wojdylo A, Figiel A, Lech K, et al. Effect of convective and vacuum-microwave drying on the bioactive compounds, color, and antioxidant capacity of sour cherries. Food Bioprocess Technol. 2014;7:829–41.
18. FAO. Food and Agriculture Organization of the United Nations. 2016. http://faostat.fao.org. Accessed 21 Aug 2019.
19. Doymaz İ. Influence of pretreatment solution on the drying of sour cherry. J Food Eng. 2007;78:591–6.
20. Damar İ, Ekşi A. Antioxidant capacity and anthocyanin profile of sour cherry (*Prunus cerasus* L.) juice. Food Chem. 2012;135:2910–4.
21. Sun SY, Che CY, Sun TF, et al. Evaluation of sequential inoculation of *Saccharomyces cerevisiae* and *Oenococcus oeni* strains on the chemical and aromatic profiles of cherry wines. Food Chem. 2013;138(4):2233–41.
22. Duran-Valle CJ, Gomez-Corzo M, Gomez-Serrano V, et al. Preparation of charcoal from cherry stones. Appl Surf Sci. 2006;252:5957–60.
23. Olivares-Marin M, Fernandez-Gonzales C, Macias-Garcia A, et al. Preparation of activated carbons from cherry stones by activation with potassium hydroxide. Appl Surf Sci. 2006;252:5980–3.
24. Angin D. Production and characterization of activated carbon from sour cherry stones by zinc chloride. Fuel. 2014;115:804–11.
25. Gonzales JF, Encinar JM, Canito JL, et al. Pyrolysis of cherry stones: energy uses of the different fractions and kinetic study. J Anal Appl Pyrolysis. 2003;67:165–90.
26. Duman G, Okutucu C, Ucar S, et al. The slow and fast pyrolysis of cherry seed. Bioresour Technol. 2011;102:1869–78.
27. Alper K, Tekin K, Karagöz S. Pyrolysis of agricultural residues for bio-oil production. Clean Technol Environ. 2015;17:211–23.
28. Özsin G, Pütün AE. Kinetics and evolved gas analysis for pyrolysis of food processing wastes using TGA/MS/FT-IR. Waste Manag. 2017;64:315–26.
29. Korlesky NM, Stolp LJ, Kodali DR, et al. Extraction and characterization of Montmorency sour cherry (*Prunus cerasus* L.) pit oil. J Am Oil Chem Soc. 2016;93:995–1005.
30. Gillespie GD, Everard CD, Fagan CC, et al. Prediction of quality parameters of biomass pellets from proximate and ultimate analysis. Fuel. 2013;111:771–7.
31. Cruz G, Rodriguez ALP, Silva DF, et al. Physical-chemical characterization and thermal behavior of cassava harvest for application in thermochemical processes. J Therm Anal Calorim. 2020. https://doi.org/10.1007/s10973-020-09330-6.
32. Chandrasekaran A, Ramachandran S, Subbiah A. Determination of kinetic parameters in the pyrolysis operation and thermal

behavior of Prosopis juliflora using thermogravimetric analysis. Bioresour Technol. 2017;233:413–22.

33. White JE, Catallo WJ, Legendre BL. Biomass pyrolysis kinetics: a comparative critical review with relevant agricultural residue case studies. J Anal Appl Pyrol. 2011;91:1–33.

34. Doyle CD. Estimating isothermal life from thermogravimetric data. J Appl Polym Sci. 1962;6:639–42.

35. Coats AW, Redfern JP. Kinetic parameters from thermogravimetric data. Nature. 1964;201:68–9.

36. Starink MJ. The determination of activation energy from linear heating rate experiments: a comparison of the accuracy of isoconversion methods. Thermochim Acta. 2003;404:163–76.

37. Friedman HL. Kinetics of thermal degradation of char-forming plastics from thermogravimetry. Application to a phenolic plastic. J Polym Sci Part C Polym Sympos. 1964;6(1):183–95.

38. Flynn J, Wall L. A quick, direct method for the determination of activation energy from thermogravimetric data. J Polym Sci Pol Lett. 1966;4:323–8.

39. Ozawa T. A new method of analyzing thermogravimetric data. Bull Chem Soc Jpn. 1965;38(11):1881–6.

40. Kissinger H. Variation of peak temperature with heating rate in differential thermal analysis. J Res Nat Bureau Stand. 1956;57(4):217–21.

41. Akahira T, Sunose T. Joint convention of four electrical institutes. Sci Technol. 1971;16:22–31.

42. García R, Pizarro C, Lavín AG, et al. Characterization of Spanish biomass wastes for energy use. Bioresour Technol. 2012;103:249–58.

43. McKendry P. Energy production from biomass (part 1): overview of biomass. Bioresour Technol. 2002;83:37–46.

44. Ceylan S, Topcu Y. Pyrolysis kinetics of hazelnut husk using thermogravimetric analysis. Bioresour Technol. 2014;156:182–8.

45. Yuakkul D, Amornsakchai T, Saikrasun S. Effect of maleated compatibilizer on anisotropic mechanical properties, thermo-oxidative stability and morphology of styrenic based thermoplastic elastomer reinforced with alkali-treated pineapple leaf fiber. Int J Plast Technol. 2015;19(2):388–411.

46. Brebu M, Cazacu G, Chirila O. Pyrolysis of lignin—a potential method for obtaining chemicals and/or fuels. Cell Chem Technol. 2011;45(1–2):43–50.

47. Lin X, Sui S, Tan S, et al. Fast pyrolysis of four lignins from different isolation processes using Py-GC/MS. Energies. 2015;8:5107–21.

48. Yang H, Yan R, Chen H, et al. Characteristics of hemicellulose, cellulose and lignin pyrolysis. Fuel. 2007;86:1781–8.

49. Lazaridis PA, Fotopoulos AP, Karakoulia SA, et al. Catalytic fast pyrolysis of kraft lignin with conventional, mesoporous and nanosized ZSM-5 zeolite for the production of alkyl-phenols and aromatics. Front Chem. 2018;6:295.

50. Li D, Briens C, Berruti F. Improved lignin pyrolysis for phenolics production in a bubbling bed reactor—effect of bed materials. Bioresour Technol. 2015;189:7–14.

51. Açıkalın K. Thermogravimetric analysis of walnut shell as pyrolysis feedstock. J Therm Anal Calorim. 2011;105:145–50.

52. Gogoi M, Konwar K, Bhuyan N, et al. Assessments of pyrolysis kinetics and mechanisms of biomass residues using thermogravimetry. Bioresour Technol Rep. 2018;4:40–9.

53. Alvarenga LM, Xavier TP, Barrozo MAS, et al. Determination of activation energy of pyrolysis of carton packaging wastes and its pure components using thermogravimetry. Waste Manag. 2016;53:68–75.

54. Alias NB, Ibrahim N, Hamid MKA. Pyrolysis of empty fruit bunch by thermogravimetric analysis. Energy Procedia. 2014;61:2532–6.

55. Pandey MP, Kim CS. Lignin depolymerization and conversion: a review of thermochemical methods. Chem Eng Technol. 2011;34(1):29–41.

56. He Z, Xia Z, Hu J, et al. Thermal decomposition and kinetics of electrically controlled solid propellant through thermogravimetric analysis. J Therm Anal Calorim. 2020;139:2187–95.

57. Liu H, Wang C, Zhao W, et al. Pyrolysis characteristics and kinetic modeling of Artemisia apiacea by thermogravimetric analysis. J Therm Anal Calorim. 2018;131:1783–92.